

Radiation effects in Zr and Hf containing garnets

Karl R. Whittle^{1,3}, Mark G. Blackford¹, Katherine L. Smith¹, Nestor J. Zaluzec², Matthew Weyland^{4,5} and Gregory R. Lumpkin¹

¹ Institute of Materials Engineering, Australian Nuclear Science and Technology Organisation, PMB1, Menai, NSW 2234, Australia

² Argonne National Laboratory, 9700 South Cass Avenue, Argonne, IL 60439, USA

³ Department of Materials Science and Engineering, University of Sheffield, Mappin Street, Sheffield, S1 3JD, United Kingdom

⁴ Monash Centre for Electron Microscopy, Monash University, Victoria 3800, Australia

⁵ Department of Materials Engineering, Monash University, Victoria 3800, Australia

Abstract

Garnets have been considered as host phases for the safe immobilisation of high-level nuclear waste, as they have been shown to accommodate a wide range of elements across three different cation sites, such as Ca, Y, Mn on the a-site, Fe, Al, U, Zr, and Ti on the b-site, and Si, Fe, Al on the c-site. Garnets, due to their ability to have variable composition, make ideal model materials for the examination of radiation damage and recovery in nuclear materials, including as potential waste forms. Kimzeyite, $\text{Ca}_3\text{Zr}_2\text{FeAlSiO}_{12}$, has been shown naturally to contain up to 30wt% Zr, and has previously been examined to elucidate both the structure and ordering within the lattice. This study examines the effects of radiation damage and recovery using in-situ ion beam irradiation

with 1 MeV Kr ions at the IVEM-TANDEM facility, Argonne National laboratory. The complementary Hf containing system $\text{Ca}_3\text{Hf}_2\text{FeAlSiO}_{12}$ was also examined, and found to have a different response to irradiation damage. A sample of irradiated $\text{Ca}_3\text{Zr}_2\text{FeAlSiO}_{12}$, at 1000K, was characterised using aberration corrected (S)TEM and found to contain discrete, nano-sized, crystalline Fe rich particles, indicating a competing process during recovery is occurring.

Introduction

Garnets, $\text{A}_3\text{B}_2\text{C}_3\text{O}_{12}$, when found naturally are generally based on silicates, for example grossular ($\text{Ca}_3\text{Al}_2\text{Si}_3\text{O}_{12}$). The garnet-structure is body-centred cubic, formally adopting $1a3d$ symmetry, with differing local co-ordinations by oxygen for each cation type, i.e. A is cubically co-ordinated, B octahedrally co-ordinated, and C tetrahedrally co-ordinated. These polyhedra order themselves topologically such that B and C polyhedra corner share alternately, giving rise to chains in the $\langle 100 \rangle$ direction, which then cross-link through B octahedra forming a three-dimensional array. The A and C polyhedra form another three dimensional array, this time with polyhedral edge-sharing, giving rise to chains of alternate A and C polyhedra along the $\langle 100 \rangle$ direction [1]. An example image is shown in Figure 1.

Natural garnets are found to include a wide range of cations, for example the mineral scholormite contains Ti^{4+} along with a range of other cations, i.e.

$(\text{Ca}_{2.87}\text{Mg}_{0.10}\text{Na}_{0.04})(\text{Ti}_{1.06}\text{Fe}_{0.69}\text{Al}_{0.14}\text{Zr}_{0.04}\text{Mg}_{0.04}\text{Mn}_{0.03}\text{V}_{0.01})(\text{Si}_{2.35}\text{Fe}_{0.65})\text{O}_{12}$. Garnets have also been shown to be capable of containing uranium, thorium and lanthanides, making them ideal as candidates for nuclear waste storage hosts.

Kimzeyite [1], [2], [3], a natural mineral with the simplified formulation $\text{Ca}_3\text{Zr}_2\text{FeAlSiO}_{12}$, has previously been examined by neutron diffraction, Mössbauer spectroscopy and electron channeling, using HAREXCS [1], determining the structure and ordering within the cationic sub-lattice. This work was extended to include modified compositions based on Zr and Hf, such as $\text{Ca}_3\text{Zr}_2\text{FeAlSiO}_{12}$ and $\text{Ca}_3\text{Zr}_2\text{Fe}_2\text{SiO}_{12}$. Two of these modified compositions were taken and irradiated at the IVEM-TANDEM facility, $\text{Ca}_3\text{Zr}_2\text{FeAlSiO}_{12}$ and $\text{Ca}_3\text{Hf}_2\text{FeAlSiO}_{12}$.

Since the structure of garnet defines the cation locations as being special positions within the unit cell, and therefore fixed, any structural modification induced from a compositional change will be visible in changes within the oxygen sub-lattice. In the systems under irradiation it has been found previously that the change in oxygen position is within experimental error, and can therefore be considered to be identical, original refinement shown in Whittle et al [1]. As a result garnets when irradiated provide an advantage not found in many other systems, with a composition change in garnet, any structural modification, in this case a slight movement within the anionic array, is negligible. Such an observation allows us to remove structure from analysis of recovery, and focus on the compositional changes, in this case Zr^{4+} to Hf^{4+} , as all other components are constant. Other systems which can utilise this approach are pyrochlores, where there is a large body of work examining compositional effects with a constant structure, and spinels, although here there is the potential issue of partial inversion.

Experimental

As outline in Whittle et al [1], the simplified samples were prepared by heating stoichiometric amounts of CaCO_3 , Al_2O_3 , Fe_2O_3 , ZrO_2 , HfO_2 , and SiO_2 at 1400°C for 48hrs

and then ground. The samples were dispersed as crushed grains on holey-carbon coated Cu grids prior to irradiation. Sample irradiation was undertaken using the IVEM-TANDEM facility at Argonne National Laboratory (ANL), the facility consists of a Hitachi 9000-NAR microscope (300 kV accelerating voltage) coupled to a Danfysik ion implanter. The irradiations were carried out using 1 MeV Kr^{2+} as the incident beam. A Gatan heating stage was used between 298 and 1050 K, and at temperatures above 600 K the powders were loaded onto holey-carbon Mo grids to minimise interaction between the grid and holder.

To minimise irradiation induced temperature effects a constant flux of 6.25×10^{11} ions $\text{cm}^{-2} \text{s}^{-1}$ was used, with the sample angled midway between the incident ion and electron beams, i.e. $\sim 15^\circ$ to the vertical. The irradiations were carried out such that either the electron beam or ion beam were interacting with the sample, preventing synergistic interactions occurring which modify the response of the sample. Multiple grains were simultaneously irradiated, with amorphisation defined as the point at which no Bragg diffraction intensities were visible in the selected area diffraction pattern, i.e. the spots disappear and only an amorphous halo is present. The average fluence required for this across all the grains being monitored is then used to define the critical fluence (F_c) for the sample at the temperature of measurement. The expected electronic and nuclear stopping powers were estimated using SRIM2012 [4], and are shown in Table 2.

The sample of $\text{Ca}_3\text{Zr}_2\text{FeAlSiO}_{12}$ irradiated at 1000 K was examined using aberration corrected TEM and STEM using a dual aberration corrected FEI Titan³, operated at 300 kV at room temperature. In TEM mode the microscope was corrected to 3rd order to 20 mrad, equivalent to 0.9 Å transfer. In STEM mode a convergence angle of 15 mrad was used, a diffraction limited probe size of ~ 1.2 Å. Annular dark field images were collected with an

inner radius of 40 mrad, leading to image contrast dominated by atomic number contrast. Chemical information was acquired by Electron energy loss spectroscopy (EELS) spectrum imaging with a collection angle of 15 mrad. A single dataset contains the Zr-M, C-K, Ca-L, O-K and Fe-L peaks. Spectrum image data were processed to produce background subtracted elemental maps, and jump ratio images.

Results and Discussion

The recorded fluences required for amorphisation at the different temperatures are shown in Table 1, and shown as the critical fluences ($\times 10^{14}$ ions cm^{-2}). The critical fluences were analysed to determine the critical temperature (T_c). The critical temperature (T_c) is defined as 'the temperature at which the rate of crystalline recovery is equal to the damage rate, and above which the samples do not amorphise', under the conditions of irradiation, in this case 1 MeV Kr^{2+} . This temperature is determined by a least squares numerical analysis of critical fluence varying with temperature [5]. The equation used as a basis for this is shown below (1), and used to determine (T_c), the critical fluence at 0 K (F_{c0}) which is inversely proportional to the damage cross section for the system under analysis, and an initial estimate of the activation energy crystalline recovery (E_a), with Boltzmann's constant (k_b) :

$$F_c = \frac{F_{c0}}{1 - \exp\left[\left(\frac{E_c}{k_b}\right)\left(\frac{1}{T_c} - \frac{1}{T}\right)\right]} \quad (1)$$

It has been reported in the literature that the energy of activation for recovery is often underestimated using this approach, and as has been suggested by Weber [6] an approach based on other non-kinetic factors is applied:

$$E_a = T_c \left[k_b \ln \left(\frac{F_{c0} \nu}{\phi} \right) \right] \quad (2)$$

This second approach uses the critical fluence at 0 K (F_{c0}), ion flux (Φ), 6.25×10^{11} ions $\text{cm}^{-2} \text{s}^{-1}$, and the effective jump frequency (ν). The effective jump frequency, ν , can itself be based on an assumption, that recovery from damage can be both thermally driven and irradiation assisted. To accommodate such an assumption E_a was calculated using values of 10^9 - 10^{12} . Changes in the estimation of ν have been found to modify the estimated actuation energy for recovery by about 20-25%. Values for T_c and F_{c0} can be estimated from the recorded data or, as in this case, obtained analysis using equation (1). The results from this analysis are shown in Table 2 and plotted in Figure 2.

The obtained critical temperatures are high when compared to some other systems, for example Zhang et al reported [7], using similar conditions of irradiation, samples which have a T_c in the range of 773 - 873 K. However, Utsunomiya et al [8, [9] in 2002, reported a different set of garnet samples, both synthetic and naturally occurring, which had a T_c range of 890 - 1130 K, with some samples having a T_c much higher. For example a natural sample of Andradite ($\text{Ca}_{3.09}\text{Fe}_{1.92}\text{Al}_{0.05}\text{Si}_{2.98}\text{O}_{12}$) had a T_c of 1030 K. A second set of reported irradiations [10], this time of samples based on Fe, and containing elements such as Ce, Zr, Gd and Th, ranged from 820-870K.

One of the key comparisons with the samples by Zhang et al [7], and the second set by Utsunomiya [8, [9] is the low level, or zero content, of Si present in the system. The samples presented here contain SiO_4 tetrahedra, ~12.5%, which when compared with those samples presented by Utsunomiya et al [8, [9] which contain SiO_4 tetrahedra in large quantities show an agreement, i.e. a high T_c .

As can be seen in the recorded, and plotted data, there seems to be a shift in T_c of $\sim 100\text{K}$ between the $\text{Ca}_3\text{Zr}_2\text{FeAlSiO}_{12}$ and $\text{Ca}_3\text{Hf}_2\text{FeAlSiO}_{12}$ systems, this shift also correlates with an increase in expected activation energy for recovery. A similar shift has been seen before, between $\text{La}_2\text{Zr}_2\text{O}_7$ and $\text{La}_2\text{Hf}_2\text{O}_7$ where the change was $\sim 220\text{K}$ [11]. The cause of this shift is not fully understood but is likely to be related to the differing orbital overlaps in Zr and Hf.

So what can be seen from the data? Firstly the T_c 's for recovery are comparable with those systems that have significant concentrations of SiO_4 tetrahedra, and that the change from Zr to Hf increases the T_c by $\sim 100\text{K}$. If one compares the structural information, and those parameters which can be predicted from structure, such as electronic and nuclear stopping factors, we can see there is not much difference between $\text{Ca}_3\text{Zr}_2\text{FeAlSiO}_{12}$ and $\text{Ca}_3\text{Hf}_2\text{FeAlSiO}_{12}$, shown in Table 2. Close examination of the predicted damage levels, taken from SRIM2013, show that there is very little difference in expected levels of damage, shown in Figure 3 and Table 3. While extrapolating such conclusions from SRIM-type simulations is complex, in these samples it does show that changing from Zr to Hf cannot account alone for the change in obtained T_c . Since structural changes cannot really explain the differences in the radiation tolerance, it must be related to changes in bonding within the structure to some other factor.

If the recorded T_c for the systems studied here are directly compared with samples of close composition but which do not contain any SiO_4 a stark contrast is found. For example the reported T_c for both $\text{Ca}_{2.4}\text{Ce}_{0.6}\text{Zr}_{2.08}\text{Fe}_{3.03}\text{O}_{12}$ and $\text{Ca}_{2.37}\text{Th}_{0.56}\text{Zr}_{2.03}\text{Fe}_{2.96}\text{O}_{12}$ are close to 850K , a significant difference from the samples reported here. As outlined above the significant SiO_4 component in these systems, $\sim 12.5\%$, has increased the T_c in

similar samples, for example those previously reported by Utsunomiya et al [9], where the levels of Si were > 20% by wt, had a T_c approaching 1140 K for N56, and 1050 K for N77.

It has been previously reported that systems with a high content of SiO_4 tetrahedra can have increased T_c 's for recovery, or they are more susceptible to amorphisation. However, this maybe based on a misconception of the recovery from damage. In nature there are multiple SiO_4 structures, found from apex-shared, to edge-shared, from tunnel to effectively closed packed. Such a wide range of structures suggests that recovery from damage for SiO_4 based garnets may not be as simple as recovering back to the initial starting material, and that other stable intermediate structures are being formed.

Secondary intermediate phases maybe forming as nano-domains of disordered material, which then grow into larger macroscopic domains, or alternatively remain nano-sized but now have a distribution of sizes. For example, secondary nano domains have been proposed by other researchers, in understanding the effects of damage on naturally occurring garnets, and in the observed damage in MAX phases (Ti_3SiC_2), and are not unknown.

Post-irradiation analysis of $\text{Ca}_3\text{Zr}_2\text{FeAlSiO}_{12}$ using aberration corrected (S)TEM highlighted a further issue which should be considered in the effects of damage on these samples. At temperatures below 1000 K the samples were found to be polycrystalline nano-sized crystallite. However, at temperature above 1000 K particles were found to have exsolved from the matrix, shown in Figure 4 and Figure 5. In Figure 4 the image was taken from a large area of sample, and showed the 'spotty' nature of the crystallites formed giving rise to a ring-type diffraction pattern showing diffuse and sharp rings, from amorphous and crystalline material respectively. High resolution aberration corrected TEM, Figure 5, shows a nanocrystalline regions embedded in the amorphous

matrix. Fourier transforms of these regions show lattice repeats consistent with BCC α -Fe". Similar reduction has been observed before in Fe containing garnets, for example Utsunomiya et al [10] found that in $\text{Ca}_3\text{Fe}_2\text{Si}_3\text{O}_{12}$, Fe^{3+} partially reduced to Fe^{2+} . However, in $\text{Ca}_3\text{Fe}_2\text{Si}_3\text{O}_{12}$ the Fe was octahedrally co-ordinated, whereas in the samples irradiated here they have been found to be tetrahedrally co-ordinated. Whether a change in crystal co-ordination has an effect on Fe stability is a matter for conjecture and cannot be answered in this work.

Such a reduction in Fe from Fe^{3+} to Fe^0 does however indicate a dramatic reduction process has occurred within the sample, leading to the conclusion that some kind of elemental partitioning has occurred. The results of the EELS spectrum imaging are presented, for exsolved and embedded nanocrystals, in Figure 6. The elemental maps of Fe, Ca and O clearly show the partitioning of the Fe into features of $\sim 5\text{nm}$ in size. The exsolved crystal clearly contains no Ca, and only a weak O signal, that peaks towards the edges of the feature. This is consistent with the growth of an Fe rich oxide around a bare α -Fe nanoparticle in air. The embedded nanocrystals are also Fe enriched and depleted in Ca and O, but due to the projection nature of TEM it is not possible to unambiguously conclude these are pure Fe. This separation of elements is indicative, if not definitive, that above 1000 K reduction of Fe^{3+} to Fe^0 occurs, but does not indicate how it occurs. There are two main possibilities for it occur one is due to electron beam damage (reduction), which while able to occur is unlikely to occur under these conditions - the electron beam is off during the irradiation process. A more likely explanation is the damage from the ion beam acting as a catalyst for reduction of Fe^{3+} to Fe^0 particularly at these high temperatures. Such a reduction mechanism modifies how the radiation damage tolerance is viewed, for example previous to the aberration corrected TEM results it would have been proposed that the garnet samples could have formed regions of nano-crystalline domains

in a broadly garnet matrix, with T_c 's in the order of 1100-1200 K. However, in light of the new results a new mechanism can be developed based on the processes involved in damage recovery.

During the initial irradiation stage, i.e. after the primary knock-on has occurred and a cascade of damage has begun, the immediate temperature of the sample is raised significantly. This immediate temperature rise rapidly decays via conduction through the sample and temperature controlled environment, however, it is still significantly high enough to take the sample above 1000 K. On recovery this damage volume then recovers to a structure that is both kinetically and thermodynamically likely, this is generally dependent on the bulk temperature of the sample. If during this process a secondary structure can be formed, for example in $ZrSiO_4$ recovery can lead to both ZrO_2 and SiO_2 forming as separate phases [8], then it is possible that discrete nano-sized volumes of secondary phases form restricting the recovery back to the initial phase. This would normally be observed as diffuse rings in selected area electron diffraction patterns, for example that found in Ti_3SiC_2 . With increasing doses of radiation these nano-sized volumes could either expand or diffuse back into the host matrix, this would depend on the stability of the structure and its ability to accommodate disorder. In effect with increasing temperature the samples would begin to react as though they were being synthesised in bulk. During the irradiation process these nanocrystalline domains, in these samples largely Fe rich, begin to grow and give rise to a sample different in composition to the initial state. Thus at temperatures above 1000 K, for where we have evidence of such a process occurring we would expect, over time, the initial compositions of $Ca_3Zr_2FeAlSiO_{12}$ and $Ca_3Hf_2FeAlSiO_{12}$ to change giving rise to a new broadly garnet composition but deficient in Fe. This new phase would then have a critical temperature for amorphisation close to that observed for $Ca_3Zr_2FeAlSiO_{12}$ and $Ca_3Hf_2FeAlSiO_{12}$.

However, at temperatures below 1000 K we would expect the compositions to remain broadly $\text{Ca}_3\text{Zr}_2\text{FeAlSiO}_{12}$ and $\text{Ca}_3\text{Hf}_2\text{FeAlSiO}_{12}$ but with the possibility of minor nano sized volumes of secondary phases.

Conclusion

Garnets based on $\text{Ca}_3\text{Zr}_2\text{FeAlSiO}_{12}$ and $\text{Ca}_3\text{Hf}_2\text{FeAlSiO}_{12}$, would normally be expected to have critical temperatures for amorphisation at 1130 and 1220 K respectively, with the potential for nano sized volumes of secondary phases being present, e.g. SiO_2 . However, at temperatures above 1000 K there is evidence to suggest that a secondary process of reduction from Fe^{3+} to Fe^0 is occurring. This change gives rise to regions of Fe metal separate to the garnet matrix, and as such modifies the recovery process. This secondary process is being investigated further and will be the subject of a future publication.

Acknowledgements

The authors thank the IVEM-TANDEM facility staff at Argonne National Laboratory (Peter Baldo and Edward Ryan), for assistance during the ion irradiation work. The IVEM-TANDEM is supported as a User Facility by the U.S. DOE, Basic Energy Sciences, under contract W-31-10-ENG-38. We also acknowledge financial support from the Access to Major Research Facilities Programme (a component of the International Science Linkages Programme established under the Australian Government's innovation statement, Backing Australia's Ability). The aberration corrected TEM and STEM EELS data was acquired on instruments within the Monash Centre for Electron Microscopy that were funded by the Australian Research Council grant number LE0454166 and Monash University.

Captions

Figure 1 - Unit cell representation of $\text{Ca}_3(\text{Zr}/\text{Hf})_2\text{AlFeSiO}_{12}$ along the 110 direction. Blue polyhedra are Ca-O, grey polyhedra are Zr/Hf-O octahedra, and green polyhedra are Fe/Al/Si-O tetrahedra. The red spheres indicate the location of O atoms.

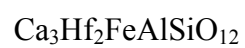
Figure 2 - Critical fluence versus temperature for $\text{Ca}_3\text{Zr}_2\text{FeAlSiO}_{12}$ and $\text{Ca}_3\text{Hf}_2\text{FeAlSiO}_{12}$, the data is fitted using Equation 1. The error bars are the average error for each recorded point taken from 5 monitored grains.

Figure 3 - Damage plots predicted by SRIM2012, simulations calculated using experimental densities, and displacement values of 50 eV for each element. The dotted lines indicate the typical thickness of sample when irradiated in a 300 kV TEM.

Figure 4 - Bright field TEM image (5000x), and recorded selected area diffraction pattern showing the sharp, but spotty nature of the rings. The rings have been indexed to Fe and show the [110], [200], and [211] diffraction intensities.

Figure 5 a) High resolution TEM image, showing nanocrystalline region, marked blue. b) Power spectrum of a), reflecting the crystal structure of the nanoparticle. Spots have been indexed assuming nanoparticle is BCC α -Fe in the [111] direction.

Figure 6 - EELS jump ratio maps for a) Exsolved nanocrystal and b) embedded nanocrystals. The last image is an RGB composite of the three maps. The jump ratios are consistent with the background subtracted elemental maps (not shown), but show higher contrast.



Temp. (K)	Fluence	Error	Temp. (K)	Fluence	Error
302	2.6	0.4	302	3.0	0.5
500	3.3	0.2	500	3.1	0.6
750	3.4	0.3	850	4.1	0.3
850	3.9	0.3	1050	7.7	2.0
1000	7.1	1.5			

Table 1 - Experimental fluences obtained from irradiation of $\text{Ca}_3\text{Zr}_2\text{FeAlSiO}_{12}$ and $\text{Ca}_3\text{Hf}_2\text{FeAlSiO}_{12}$, all fluences are presented as 10^{14} ions cm^{-2} .

System	T _c (K)	F _{Co} (ions cm ⁻²)	E _a (eV) – Eqn 1	E _a (eV) – Eqn 2	ENSP
Ca ₃ Zr ₂ FeAlSiO ₁₂	1129(49)	2.9 (0.25)	0.40 (0.15)	3.2-3.9	0.74
Ca ₃ Hf ₂ FeAlSiO ₁₂	1221(9)	3.0 (0.34)	0.32 (0.02)	3.5-4.2	0.69

Table 2 - Results obtained from the fitting of the recorded using eqn (1) and (2). The numbers in brackets are the estimated errors arising from the least squares fitting. ENSP refers to the ratio of electronic to nuclear stopping powers, as predicted by SRIM2012.

References

1. K. R. Whittle; G. R. Lumpkin; F. J. Berry; G. Oates; K. L. Smith; S. Yudintsev; N. J. Zaluzec, *Journal of Solid State Chemistry* 2007, 180, (2), 785-791.
2. C. Milton; B. L. Ingram; L. V. Blade, *American Mineralogist* 1961, 46, (5 and 6), 533-548.
3. E. Schingaro; F. Scordari; F. Capitanio; G. Parodi; D. Smith; A. Mottana, *European Journal of Mineralogy* 2001, 13, (4), 749.
4. J. Ziegler; M. Ziegler; J. Biersack, *Nuclear Instruments & Methods In Physics Research Section B-Beam Interactions With Materials And Atoms* 2010, 268, 1818-1823.
5. S. Wang; L. Wang; R. C. Ewing; R. Doremus, *Journal of Applied Physics* 1997, 81, (2), 587-593.
6. W. J. Weber, *Nuclear Instruments & Methods In Physics Research Section B-Beam Interactions With Materials And Atoms* 2000, 166-167, 98-106.
7. J. Zhang; T. S. Livshits; A. A. Lizin; Q. Hu; R. C. Ewing, *Journal Of Nuclear Materials* 2010, 407, (3), 137-142.
8. S. Utsunomiya; L. M. Wang; R. C. Ewing, *Nuclear Instruments & Methods In Physics Research Section B-Beam Interactions With Materials And Atoms* 2002, 191, 660-605.
9. S. Utsunomiya; L. Wang; S. V. Yudintsev; R. C. Ewing, *Journal Of Nuclear Materials* 2002, 303, 177-187.
10. S. Utsunomiya; S. V. Yudintsev; R. C. Ewing, *Journal Of Nuclear Materials* 2005, 336, (2-3), 251-260.
11. G. R. Lumpkin; K. R. Whittle; S. Rios; K. L. Smith; N. Zaluzec, *Journal Of Physics-Condensed Matter* 2004, 16, (47), 8557-8570.